ACSNANO
www.acsnano.org
ARTICLE

Polymer Composite with Carbon Nanofibers Aligned during Thermal Drawing as a Microelectrode for Chronic Neural Interfaces

Yuanyuan Guo,*[,†,‡] Shan Jiang,[‡] Benjamin J. B. Grena,[§] Ian F. Kimbrough,[∥] Emily G. Thompson,[∥] Yoel Fink,[§] Harald Sontheimer,[∥] Tatsuo Yoshinobu,[†] and Xiaoting Jia*[,‡]

[†]Department of Biomedical Engineering, Tohoku University, Sendai, Miyagi 9808579, Japan

[‡]Bradley Department of Electrical and Computer Engineering, Virginia Polytechnic Institute and State University, Blacksburg, Virginia 24060, United States

[§]Department of Material Science and Engineering, Massachusetts Institute of Technology, Cambridge, Massachusetts 24139, United States

[∥]Virginia Tech Carilion Research Institute, Roanoke, Virginia 14016, United States

Supporting Information

ABSTRACT: **Microelectrodes provide a direct pathway to investigate brain activities electrically from the external world, which has advanced our fundamental understanding of brain functions and has been utilized for rehabilitative applications as brain−machine interfaces. However, minimizing the tissue response and prolonging the functional durations of these devices remain challenging. Therefore, the development of next-generation microelectrodes as neural interfaces is actively progressing from traditional inorganic materials toward biocompatible and functional organic materials with a miniature footprint, good flexibility, and reasonable robustness. In this study, we developed a miniaturized all polymer-based neural probe with carbon nanofiber (CNF) composites as recording electrodes *via* the scalable thermal drawing process. We demonstrated that *in situ* CNF unidirectional alignment can be achieved during the thermal drawing, which contributes to a drastic improvement of electrical conductivity by 2 orders of magnitude compared to a conventional polymer electrode, while still maintaining the mechanical compliance with brain tissues. The resulting neural probe has a miniature footprint, including a recording site with a reduced size comparable to a single neuron and maintained impedance that was able to capture neural activities. Its stable functionality as a chronic implant has been demonstrated with the long-term reliable electrophysiological recording with single-spike resolution and the minimal tissue response over the extended period of implantation in wild-type mice. Technology developed here can be applied to basic chronic electrophysiological studies as well as clinical implementation for neuro-rehabilitative applications.**

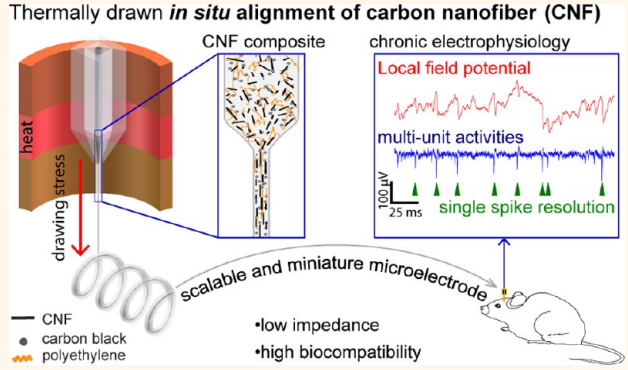

KEYWORDS: *in situ aligned carbon nanofibers, thermal drawing process, polymer composites, neural probes, in vivo chronic electrophysiological recording*

Fully understanding how the brain functions relies on deciphering the interactions between neurons; therefore, it is of great importance to develop technologies that allow monitoring of specific neurons within the investigated circuits at the single-spike and single-unit resolution during behavior. Electrical recordings, which emerged in 1930s from Edgar Adrian's work,[1] are one of the most documented technologies for this purpose, and the underlying physical principles have been well understood ever since. Such recordings detect extracellular action potentials as well as superimposed synaptic activities of neurons in the form of local field potentials (LFPs). Nowadays, within the neuroscience community, the widely adopted technologies for conducting electrical recordings are metal-based microwires[2−4] and silicon-based multichannel arrays.[5−7] These platforms have demonstrated their capabilities for recording signals from a group of neurons with single-unit resolution and high signal-to-noise

Received: November 9, 2016
Accepted: June 1, 2017
Published: June 1, 2017

DOI: 10.1021/acsnano.6b07550
ACS Nano XXXX, XXX, XXX−XXX

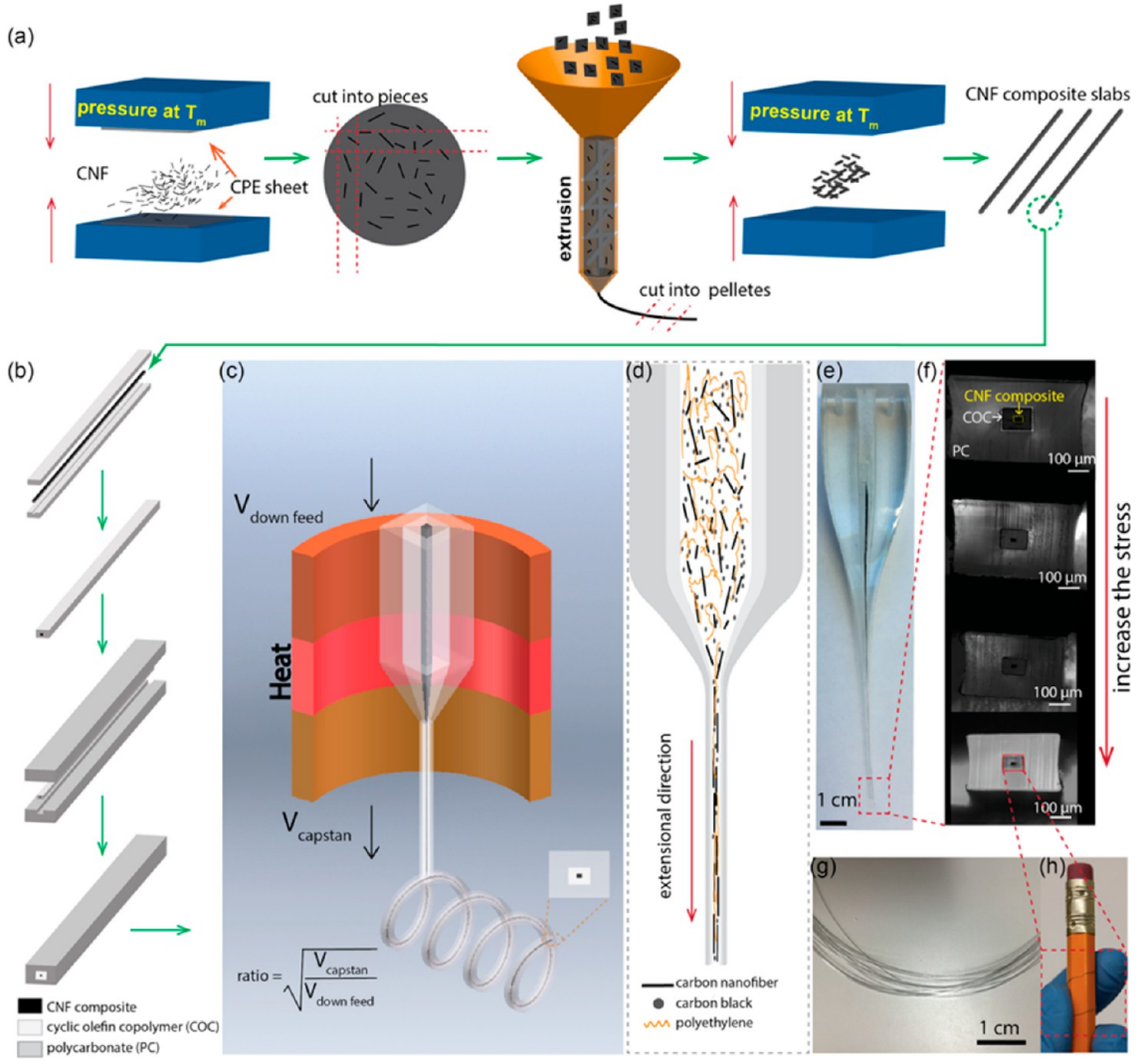

Figure 1. Fabrication of the CNF composite and fibers. (a) A schematic illustrating synthesis process for the CNF composite. (b) Fabrication process of preform including CNF composite in the center as an electrode, COC as a dielectric layer and PC as a supportive sacrificial cladding. (c) An illustration of the fiber drawing process. The dimensions of the resulting fiber were determined by the ratio of the capstan and feed speed. (d) A diagram illustrating the mechanism of the *in situ* alignment of the CNF during thermal drawing. (e) Photograph of the neck-down region showing the preform-to-fiber transition. (f) A range of cross-sectional microscope images of the drawn fiber produced by increasing the stress. (g) Photograph of the drawn fiber. (h) Photograph of the drawn fiber after the removal of the PC cladding.

ratio,[4,8,9] thanks to their miniaturized size and the low impedance characteristics of the materials. However, the severe incompatibility of these platforms with brain tissues in terms of their mechanical and biological properties[10−12] induces foreign body responses causing glial encapsulation of the probes and neuronal death, leading to extremely limited functionality for long-term chronic implantation. Therefore, there is a great interest in developing microelectrode technologies that can serve as chronically functional neural probes with miniature footprints for *in vivo* electrophysiological recording, which also meet the requirement of flexibility, biocompatibility, and robustness.[13,14]

Emerging technological trends have focused on improving brain−probe interfaces *via* surface modification of existing well-established neural probes,[10,15−21] continuous miniaturization, and the advancement of fundamental biomaterial designs.[22,23] Implantable microelectrode probes are inserted into the brain and are in direct contact with delicate brain tissues, where the initial insertion may induce disruption of glia networks. The mechanical properties, biological compatibility, and surface chemistry of the materials determine the tissue response and the implant success. The miniaturized neural probe can reduce the initial insertion damage, but the impedance of the electrode is compensated. In addition, chronic failure of silicon- and metal-based electrodes arise from elastic mismatch between the neural probes and neural tissue due to micromotion, corrosion occurring at the electrode surface, as well as the electrode fouling by gliosis, density loss of surrounding neurons, or the adsorption of proteins. Many attempts have been made to adapt the electrode design by modifying the tip geometry and surface roughness[19,21] and adopting various compliant coatings including conductive polymers (*e.g.*, poly(3,4-ethylenedioxythiophene) (PEDOT)),[15,16,18,22,24] inert metals (*e.g.*, Au, Pt), and carbon-based materials,[15−17,20] biomolecules,[25] or even live cells,[26] in order to lower the impedance, prolong their functional duration, and elicit less tissue response. Moreover, exploiting the mature planar lithography[27−30] and microcontact printing method[31−33] have enabled highly innovative neural

DOI: 10.1021/acsnano.6b07550
ACS Nano XXXX, XXX, XXX−XXX

probes such as the work reported by T. Kim *et al.*[33] and C. Xie *et al.*[28] Microelectrodes and interconnects with several micron thickness can be defined on the flexible polymer substrate, such as polyimide or SU-8 polymer layers. These flexible, foldable organic and hybrid electronics address the elastic issues, can be introduced deep in the brain through the releasable injection microneedles,[33] capillary syringe needles,[27,29,30] or stereotaxically implanted after rapid freezing in liquid nitrogen.[28]

However, fundamental advancement of biomaterials is the ultimate solution for addressing the aforementioned issues and extending the electrical intervention duration for clinical applications. One possibility is to develop flexible, biocompatible, and electrically conductive organic materials. Takashi D. Y. Kozai *et al.* reported a single carbon fiber-based microelectrode with bioactive surface of PEDOT, which had a footprint of <10 μm in diameter, yet maintained superior electrical characteristics for chronic recording with high fidelity.[22] The preliminary biocompatibility of this microelectrode was demonstrated over 2 weeks of implantation. However, the main hindrance for the wide application of this device was the complication of the device assembly based on a single carbon fiber and the lack of robustness of the implant, as the headcap was subjected to fail after several weeks. In addition, a large-scale recording *via* integrating multiple recording units could be problematic. Andres Canales *et al.* developed polymer-based multifunctional fibers using a thermal drawing process, allowing for the study of brain activities across its different signaling mechanisms.[34] In these probes, polyethylene was incorporated with carbon particles (*i.e.*, conductive polyethylene (CPE)) as the chosen electrical recording material, which is commercially available as an electronic packaging material. These probes have demonstrated their excellent chronic performance and biocompatibility over 3 months of implantation. However, due to the low conductivity of this composite, the recording site had to be sufficiently large to maintain moderate impedance for recording spike activities. Therefore, the resulting implantable fiber probes had large footprints that induced considerable insertion tissue damage. Though these innovations in both material designs and probe fabrication have boosted the development of the next generations of microelectrode technologies, the results rendered by the balances between size, conductivity, biocompatibility, and robustness are not yet satisfying.

In this study, we report the fabrication of a polymer composite fiber with the carbon nanofiber (CNF) aligned *in situ* during the thermal drawing. The resulting neural probe, based on this flexible composite fiber, has stable electrical recording performance and high biocompatibility over the chronic implantation. CNF and carbon nanotube (CNT) are both commonly explored fillers to create a composite because of their high aspect ratio that contributes to the improvement of electrical conductivity. However, in this study, CNF is chosen for its low cost, high-biocompatibility,[35−37] and mainly for its stacked-cup morphology. This morphology generates exposed reactive edge planes along the entire interior and exterior surfaces facilitating rapid electron charge transfer. The composite is made of 2 vol % CNF (Prograf Product, Inc.) impregnated into CPE (Hillas Packaging). CPE was chosen as a result of its base conductivity from carbon black particles embedded in the polymer matrix and its reported long-term biocompatibility. At higher loading of CNF, the viscosity at the processing temperatures was too high to be compatible with commonly drawn thermoplastic polymers. Figure 1a shows the synthesis process for the CNF composite. The CNF was first embedded into the CPE sheet by compression with heat, and then CNF composite with a homogeneous loading of CNF was achieved by following an extrusion process of pressed CPE and CNF. After the material synthesis, a rectangular macroscopic preform was prepared. It had the CNF composite in the center, which was surrounded by cyclic olefin copolymer (COC) as a dielectric layer and a subsequent polycarbonate (PC) cladding as a sacrificial layer that would be removed after the thermal drawing. The schematic model is shown in Figure 1b. Then this preform was thermally drawn into hundreds of meters long fibers with a conserved cross-sectional geometry and composition, but with a much reduced size defined by the draw-down ratio as shown in Figure 1c. Figure 1d illustrates the mechanism of *in situ* alignment of CNF occurring during the thermal drawing. The randomly oriented CNFs within the composite are reoriented by the elastic field from the polymer matrix along the extension, resulting in an increase of the electrical conductivity in the longitudinal direction. Figure 1e shows the neck-down region of the preform-to-fiber transition demonstrating the scalability of the thermal drawing process, which produces fibers in Figure 1g with high yield. Their cross-sectional areas can be tuned by the drawing stress, but the geometry is maintained as shown in Figure 1f. A higher drawing stress can result in a fiber with smaller dimensions. After removing the PC sacrificial layer, the resulting fiber had overall dimensions of <100 μm × 100 μm including a recording site of CNF composite with a size ranging from 18.0 μm × 11.3 to 35.2 μm × 20.1 μm. The fiber was mechanically flexible as shown in Figure 1h. Its capability for both acute and chronic recording, along with biocompatibility, in the wild-type mice was demonstrated.

RESULTS AND DISCUSSION

Characterization *via* Scanning Electron Microscope (SEM). The material properties of the CNF composite were characterized by SEM (LEO (Zeiss) 1550 field-emission SEM). Samples of CNF composite prior to the thermal drawing were freeze-fractured with liquid nitrogen and imaged *via* SEM. A random orientation of CNFs was confirmed as shown in Figure 2a. A slight tendency toward a certain orientation may be due to hot compression. Similarly, cross sections of the drawn fibers were prepared by liquid nitrogen fracture and imaged *via* SEM as shown in Figure 2b. The CNFs stand out perpendicularly to the electrode cross-sectional surface, indicating the high possibility of the alignment along the longitudinal direction. To further investigate the alignment, the drawn fiber underwent selective etching processes, in which the PC sacrificial layer was etched by dichloromethane (Sigma-Aldrich), and the COC dielectric layer was etched by toluene (Sigma-Aldrich), which left only the drawn CNF composite as shown in Figure 2c. The observed CNFs are aligned longitudinally in Figure 2c-ii and c-iii. As this observed alignment occurs on the exposed surface, which was at the interface between the composite electrode and COC dielectric layer, it could stem from the sheer force attributed to difference in viscosity from two materials during the thermal drawing process.

Validation of CNF Alignment *via* Focused Ion Beam (FIB) Technique. In order to validate the alignment of the CNF in the bulk composite, FIB technique was utilized (FEI Helios 600 NanoLab). Here CNF fiber samples drawn at the lowest stress were prepared, since the alignment in the bulk is essentially induced by the drawing stress. If the substantial alignment in the CNF composite is achieved at the lowest

DOI: 10.1021/acsnano.6b07550
ACS Nano XXXX, XXX, XXX−XXX

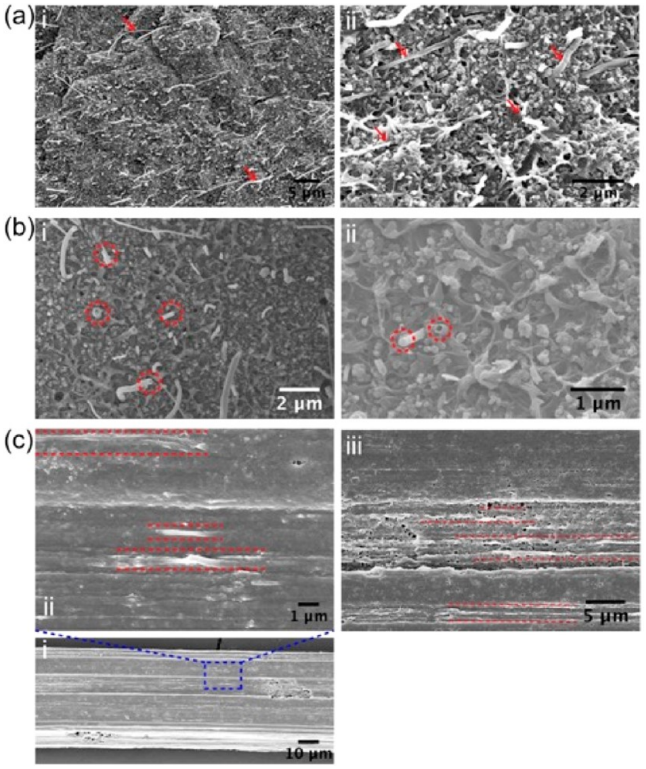

Figure 2. Material characterizations *via* SEM. (a) SEM of the CNF composite before thermal drawing. (a-i and a-ii) Random CNF orientation observed on the fractured surface at different magnifications. Red arrows point to some examples of CNFs. (b) SEM of the fractured cross-section of the drawn CNF composite. (b-i and b-ii) CNFs standing out from the cross-section of the composite at different magnifications; the examples of which are illustrated by the red dashed circles. (c) SEM of the etched composite electrode. (c-i) Exposed longitudinal surface of CNF composite after removing the PC and the COC. (c-ii and c-iii) Aligned CNF on the surface of the composite as indicated by the red dashed lines.

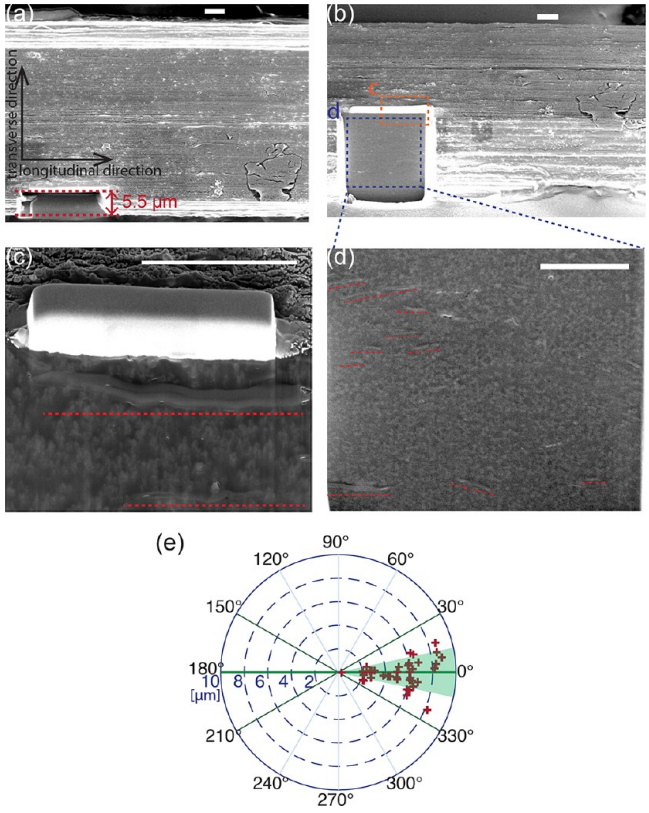

Figure 3. Milling of the CNF composite *via* FIB. (a) SEM showing the milling depth of the CNF composite in its transverse direction. (b) SEM indicating exposure area at the irradiation angle of 52° after the completion of milling. (c) Zoom-in SEM in the course of milling at the irradiation angle of 52° showing the platinum (Pt) deposition and two aligned CNFs as indicated by the red dashed line. (d) SEM of the exposed area during the final polish milling at the irradiation angle of 52° with multiple aligned CNFs as indicated by the red dashed line. More images of the exposed areas showing aligned CNFs during the course of FIB milling are shown in Supplementary Figure 3. (Scale bar: 5 μm.) (e) The polar plot with angle of the exposed CNF with respect to the longitudinal direction and the radius defined as the distance of the exposed CNF to the surface. The green area is the angle zone smaller than 10°, and most of the exposed CNFs fall into this area showing substantial alignment.

drawing stress, in this case it is about 80 g/mm^2 (drawing conditions shown in the Supplementary Figure 1), then a higher degree of alignment is expected with a higher drawing stress, thus, it can confirm the alignment of the CNF in the bulk composite throughout the entire drawn fiber.

A thin layer of platinum (Pt) was first deposited on top of the region of interest to elicit less "curtain effect" and less charging issues on newly exposed areas. Then a three-step gallium (Ga) ion milling process from rough milling to fine milling took place by varying the ion current from 0.92 nA to 0.28 nA to eventually 93 pA at the final polish step. Figure 3a shows SEM of the composite electrode taken at a nontilted angle, indicating that the electrode was milled 5.5 μm deep into its transverse direction. Figure 3b shows the exposed inner area (18 μm × 19 μm) of the electrode after the final polish. Figure 3c–d depicts the areas containing aligned CNFs during the milling process. Figure 3c shows the deposited Pt strip on the top of the electrode surface below where the milling process took place and two CNFs orienting in the longitudinal direction were exposed. Furthermore, Figure 3d shows the tendency of longitudinal orientation of CNF by exposing regions with multiple CNFs orienting to their extensional direction.

Quantitative assessment of the alignment was also performed as demonstrated in the polar plot in Figure 3e. The angle is defined as the exposed individual CNF with respect to the longitudinal direction, and the radius indicates the distance between the CNF and the electrode surface. In this set of the experiments, there were 41 CNFs exposed, and 28 of were in the area with an angle smaller than 10°, and all have angles smaller than 30°. It demonstrates that the substantial alignment in the bulk was achieved when a stress of 80 g/mm^2 was applied. A tendency of higher degrees of alignment is observed in the individually exposed CNF near the surface, which could result from the dual effect of the shear force at the surface and the drawing stress. In addition, alignment was further evaluated by measuring the resistivity of the CNF composite drawn under different stresses. It was observed that a lower resistivity was achieved at a higher drawing stress, which demonstrated greater drawing stresses induce higher degrees of alignment (shown in Supplementary Figure 5). The results obtained from the FIB milling confirm our hypothesis and demonstrate that CNFs are

DOI: 10.1021/acsnano.6b07550
ACS Nano XXXX, XXX, XXX−XXX

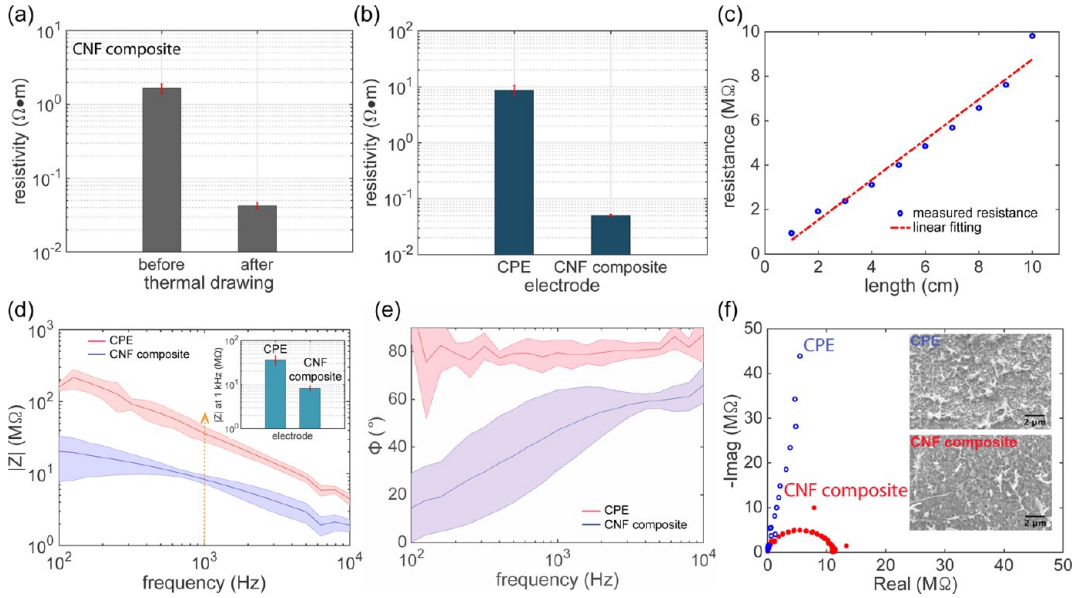

Figure 4. Electrical characterization of the CNF composite. (a) Comparison of the resistivity of CNF composites before and after the thermal drawing process indicating a significant reduction in the resistivity attributed to *in situ* unidirectional alignment of the CNF during thermal drawing. (b) Comparison of the resistivity between the thermally drawn CPE and CNF composite indicating a drastic improvement of electrical conductivity of the composite with aligned CNF compared with the conventional CPE. (c) Measurement of the resistance of the thermally drawn CNF composite *versus* its length showing their linear relationship ascribed to the homogeneous distribution and alignment of CNFs. (d) The Bode magnitude impedance plot of the CPE and CNF composite electrode showing the low impedance characteristics of the CNF composite. (e) The Bode phase impedance plot of the CPE and CNF composite showing the less capacitive behavior of the CNF composite. (f) The Nyquist plot of the CPE and CNF impedance (10 Hz to 10 kHz), indicating that the CNF has a semicircle feature dominated by the faradaic current. All error bars and shaded areas in the figure represent standard deviation.

aligned not only at the interface between composite and COC but also within the CPE during the thermal drawing process.

Electrical Characterization of the CNF Composite. CNF is known to have good electrical conductivity;[35,36] thus the composite with unidirectionally aligned CNF is expected to further improve its electrical characteristics, which makes it a suitable microelectrode material for electrophysiological recording. The comparison of the resistivity of CNF composite before and after thermal drawing was conducted *via* a probing station (Keithley 4200SCS Parameter Analyzer). The CNF composite slabs prior to the thermal drawing with defined dimensions (cross-section of 0.52 mm × 2.0 mm, length from 4 cm to 1 cm) were prepared by low-end machining. Thermally drawn fiber sections with lengths ranging from 10 cm to 1 cm with the CNF composite of the cross-sectional size of 23 μm × 18 μm were also prepared. The resistivity results are shown in Figure 4a. There is almost a 40-fold reduction in the resistivity of the thermally drawn CNF composite (0.043 Ω·m) compared to the CNF composite prior to the thermal drawing (1.65 Ω·m), which we attribute to the longitudinal *in situ* alignment of CNF that occurred during the thermal drawing process.

To compare the electrical conductivity with conventionally used carbon-based polymer composite, *e.g.*, CPE, fibers with CPE electrode were also drawn to serve as a comparison. Fiber sections of CNF composite and CPE with lengths of 1 cm and similar cross-sectional sizes (25.7 μm × 16.6 μm and 37.2 μm × 14.6 μm, respectively) were prepared, and their resistivities were measured. The results are shown in Figure 4b, in which a significant reduction of the electrical resistivity of the CNF composite (0.05 Ω·m) by 2 orders of magnitude was observed compared with the conventional CPE (8.72 Ω·m), due to the alignment of the CNF.

To evaluate the homogeneous alignment and distribution of CNFs, CNF composite fiber with a length of 10 cm produced at the maintained drawing stress was prepared, and its DC resistance was measured. Then it was shortened in 1 cm increments, and the resistance was measured accordingly. The results are plotted as resistance *versus* length in Figure 4c. A close linear correspondence was observed, which suggested the uniform distribution and alignment of CNFs within the composite at maintained drawing stress.

To explore the possibility of its application as an implantable microelectrode for neural recording, its electrochemical impedance characteristics were evaluated *via* electrochemical impedance spectrum (EIS) (Interface 1000E, Gamry Instruments). Measurements adopted the schemes of a three-electrode setup, which consisted of a 2 cm-long fiber with CNF composite or CPE electrode with similar cross-sectional areas as a working electrode (Supplementary Figure 6), a Ag/AgCl reference electrode, and a Pt wire as a counter electrode. Bode plots of the impedance spectra are shown in Figure 4c–d. The Bode magnitude impedance plot shows a significant decrease in the impedance of the CNF composite compared with the CPE at all frequencies, especially at 1 kHz, a frequency of interest for electrophysiological recording with single-spike resolution. The Bode phase impedance plot demonstrates a more faradaic CNF composite interface, which is dominated by the electron-transfer resistance at low frequencies and exhibits a greater capacitive behavior at higher frequencies. This phenomenon was further confirmed by the Nyquist plot as shown in Figure 4f. The CNF composite exhibits semicircle features which can be easily modeled *via* a simplified Randle cell attributed to the surface electrochemistry, while the CPE shows nonsemicircle features. All the plots were recorded in the frequency range from 10 Hz to 10 kHz. This distinct

DOI: 10.1021/acsnano.6b07550
ACS Nano XXXX, XXX, XXX−XXX

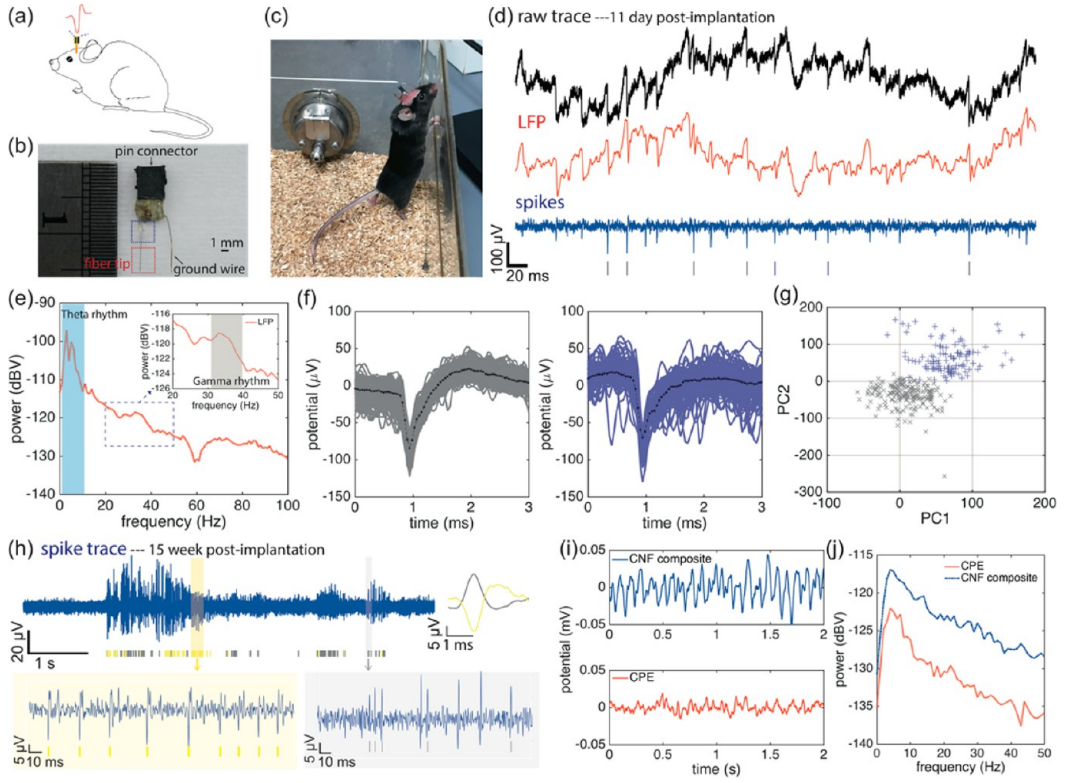

Figure 5. ***In vivo*** **electrophysiological experiments. (a) A schematic of implantation. (b) Photograph of the assembled neural probe with fiber tip for insertion after removing the PC layer. (c) Photograph of a wild-type mouse with chronically implanted neural probe in the hippocampal formation. (d) Recorded electrophysiological signal following 11 days of implantation. Top trace shows the unfiltered signal, middle trace shows bandpass-filtered (0.3−300 Hz) LFP, and the bottom trace represents the bandpass-filtered (0.5−5 kHz) spike trace with detected spike timing relative to the simultaneously recorded LFP from the same electrode (color coded). (e) Power spectral density analysis of the LFP revealing the θ and γ oscillations. (f) Two clustered single-unit action potentials with their average waveform shown as black dotted line. (g) PCA demonstrating good isolation of the two clusters. (h) Recorded spike trace following 15 weeks of chronic implantation, from which two units could still be well isolated with their average waveforms displayed at the end of the traces and spike timing indicated in the trace (color coded). Two representative traces reveal the spontaneous activities from two single units in detail. Unclustered spikes are not shown. (i) A section of raw LFPs recorded from neural probes with the CNF composite and CPE electrodes on day 0 showing difference in the amplitude of brain oscillations. (j) Power spectral density across the LFP range indicating that both materials can capture the brain oscillations at low frequencies, but the CNF composite improves the power density from −122 dBV to −117 dBV in the frequency range of interest (≤12 Hz).**

characteristic of the electrochemical impedance of the CNF composite can be explained by the high aspect ratio and the stacked-cup CNF morphology, which generates large amounts of exposed edge sites along both the interior and exterior surfaces. This facilitates rapid electron-transfer kinetics at the electrode−electrolyte interface and thus elicits less capacitive behavior, which results in a predominant faradaic interface and is suitable for picking up neural signals at both a high- and low-frequency range of interest. In contrast, the CPE has a mainly capacitive behavior across all measured frequencies, which is mainly due to the capacitance existing in the thermally drawn CPE from carbon particles embedded within the elongated polyethylene polymer matrix (Supplementary Figure 6).

In Vivo **Electrophysiology.** A neural probe was assembled from this CNF composite fiber by straightforward customization of connecting it with headpins. Fiber sections having cross-sectional dimensions in the range from 18.0 μm × 11.3 to 25.7 μm × 16.6 μm were chosen. It was implanted into the hippocampal formation of wild-type mice for electrophysiological experiments as shown in Figure 5a−b (N = 10). Figure 5c shows a CNF composite fiber-based neural probe implanted into a wild-type mouse for over 1 month. Chronic electrophysiological recordings were performed *via* Tucker-Davis Technologies (TDT) Neurophysiological Systems.

Electrophysiological signals, revealing the LFP (0.3−300 Hz) and spike activities (0.5−5 kHz) in Figure 5, were recorded at 11 days after the implantation in Figure 5d. Power spectral density analysis of the LFP in Figure 5e shows brain oscillations were observed in the range of 5−10 Hz and 30−40 Hz, which correspond to the θ and γ bands of hippocampal network patterns of activity in a mouse.[38−40] The spiking trace shows that our CNF composite probe can record spiking activities from multiple neurons that are close to the probe with single-spike resolution. From them, two representative spike clusters could be sufficiently isolated from our recording *via* the principal component analysis (PCA), and their detected spike timings are indicated in the trace. The quality of the isolation between single units was assessed by calculating two standard metrics: the L-ratios and isolation distance (0.0081 and 78.7, respectively). Clusters with an L-ratio <0.2 and an isolation distance >20 were considered well-separated single units.

After 15 weeks of implantation, the same CNF composite probe was still able to capture electrophysiological signals of multi-unit activities with single-spike precision, as shown in Figure 5h. The spike trace demonstrates its capability of

DOI: 10.1021/acsnano.6b07550
ACS Nano XXXX, XXX, XXX−XXX

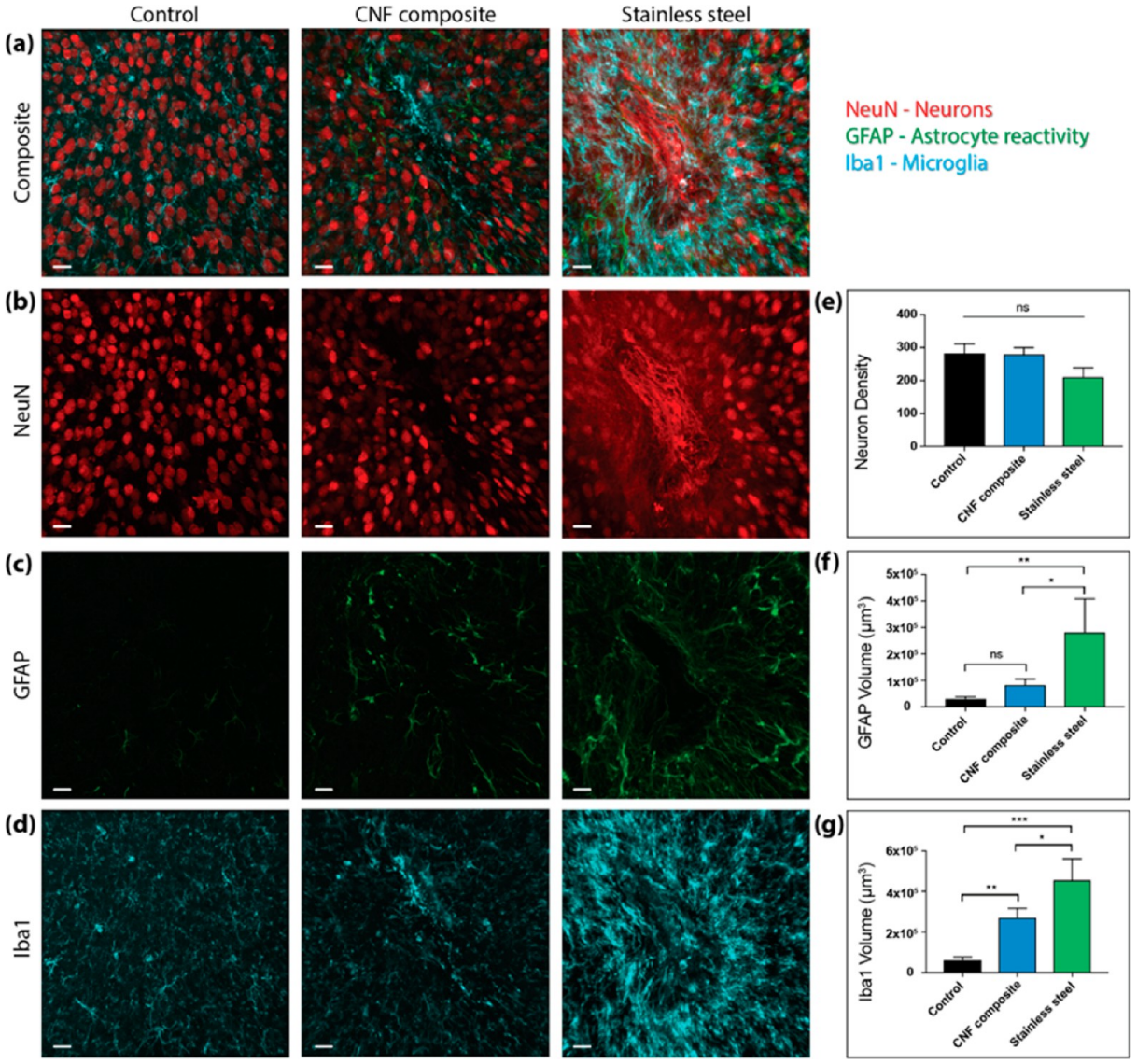

Figure 6. Histological comparison of tissue reaction to chronically implanted CNF composite probes and conventional stainless steel probes following a 4 week implantation. Control images were acquired from the contralateral side of the implanted brain. (a−d) Z-projections created from confocal optical sections. Neurons were labeled with NeuN (red), astrocytes were labeled with GFAP (green), and microglia were labeled with Iba1 (Cyan). (a,e) Neuron density, calculated by counting NeuN labeled neurons, was not significantly different between the groups. (c,f) Astrocyte reactivity, measured as the volume of GFAP-positive cells, was significantly increased (p = 0.0314) in the tissue implanted with a stainless steel probe compared to the CNF composite probe. (d,g) The volume of Iba1-positive cells was also significantly increased (p = 0.0291) in the tissue implanted with a stainless steel probe compared to the CNF composite probe. Significance was determined by one-way ANOVA with Holm−Sidak's multiple comparison test. Error bars on bar graphs reflect the standard error of the mean; * represents statistical significance with a P-value <0.05, ** P < 0.01, *** P < 0.001. (Scale bar: 20 μm.)

recording spontaneous activities from adjacent neurons, from which two clusters could be well-isolated with their average waveform displayed at the end of the trace and their spike timing indicated in the two representative trace. Thus, recording performance of the CNF composite probe over extended chronic implantation was still maintained and reliable. Due to the micromotion of the neural tissue from the heartbeat, respiration, and movement of the subject mice, the probe might not record from the same neuron after prolonged implantation.

To evaluate the recording performance between the CNF composite and CPE, a neural probe made of conventional CPE fiber with similar electrode size was assembled and implanted into the hippocampal formation of the mice (N = 3). Figure 5h shows the recorded LFP obtained from fibers with the CNF composite and CPE electrodes, respectively, which captured the low-frequency event of superimposed synaptic neural activities. These two recordings were both obtained when the mice were under anesthesia at the time of surgical implantation and indicate that recording from the CNF composite has a much higher amplitude than the recording from the CPE. Their power spectral density was analyzed, as shown in Figure 5i, in which the θ-band (4−12 Hz) brain oscillation was captured by both electrodes. But the power density from neural probe based on CNF composite electrode was much increased compared with the one from the CPE electrode, especially at the frequency range of the θ band, where an improvement of 5 dBV was achieved. Furthermore, single neural probes assembled with both CNF composite and CPE electrodes with similar size

DOI: 10.1021/acsnano.6b07550
ACS Nano XXXX, XXX, XXX−XXX

were implanted into the mice (N = 3). Simultaneous electrophysiological recordings from two electrodes were performed; CNF composite electrode can record multiunit activities that resolve the individual spikes, while the CPE was not able to capture the spike activities (shown in the Supplementary Figure 11).

These results demonstrate the capability of our probe to be inserted into precise brain regions and record high-quality neural activities from neurons adjacent to the electrode over extended periods of chronic implantation.

Biocompatibility of the CNF Composite Neural Probe. To evaluate the biocompatibility of our CNF composite neural probe, we used immunohistochemical analysis of brain tissue from mice implanted for 4 weeks with either the CNF composite probe with a footprint <100 μm × 100 μm or a conventional stainless steel microwire probe with a diameter of 125 μm. The neuron-specific protein NeuN was used to analyze neuronal density, the presence of glial fibrillary acidic protein (GFAP) was used to investigate an astrocytic response to the probe, and last ionized calcium-binding adaptor molecule 1 (Iba1) was used as a morphological marker of microglial activation. Representative images from the contralateral side of an implanted brain (control), CNF composite probe, and stainless steel probe are presented in Figure 6a–d.

Neuronal density was compared between all groups, and no significant difference was observed as shown in Figure 6e. Astrocyte reactivity, measured as the volume of GFAP-positive cells, was also significantly increased (p = 0.0314) in the tissue implanted with a stainless steel probe compared to the CNF composite probe, as shown in Figure 6f. The volume of Iba1-positive cells was found to be significantly increased (p = 0.0291) between the stainless steel probe and the CNF composite probe, as shown in Figure 6g.

These results suggest that the CNF composite neural probe is biocompatible with the surrounding brain tissue. Overall, our probe displays a decreased foreign body response in brain tissue, when compared to the conventional stainless steel probe. These results solidify the applicability and potential for therapeutic implementation of our CNF composite probe at neural interfaces.

CONCLUSION

This study reported the development of a miniaturized all-polymer neural probe fabricated using a high-throughput method, *i.e.*, thermal drawing process, with advanced features of *in situ* alignment of the CNF within the composite during the thermal drawing for reliable chronic recordings. This newly developed polymer composite with CNF alignment has an electrical conductivity of 20 S/m, which is an improvement by orders of magnitude compared to that of the conventional carbon-based polymer composite. In addition, thanks to this scalable fabrication process, the resulting neural probe has an overall size of <100 μm × 100 μm, a large size reduction when compared to the conventional bulky polymer neural probes. It has a recording site down to 18.0 μm × 11.3 μm, which is comparable to the size of a single neuron but still could record high-quality neural activities from which reliable single-unit activities can be detected. The carbon-based polymer composite has long been proved to have biocompatibility over extended periods of implantation,[24,34−37] and a further evaluation of functional performance of our neural probes with the CNF composite electrodes during chronic implantation has demonstrated its stable electrophysiological recording with high fidelity and minimally evoked foreign body response. Therefore, the development of this thermally drawn fiber with *in situ* aligned CNF composite could advance the microelectrode technology fundamentally. As thermal drawing is a versatile fabrication process, in the future, a large-scale recording can also be readily achieved by fabricating a fiber with an array of CNF composite electrodes. It can be realized by bundling fibers with CNF composite electrodes together and undergoing another round of thermal drawing. The resulting CNF composite array can have a single electrode size down to submicron or even nanoscale without the need of high-precision fabrication methods, and also it is expected to realize a further alignment of single CNF following steps of thermal drawing. Additionally, this CNF composite can be functionalized with specific enzymes to provide analytic specificity that could realize direct neurochemical sensing.[35,41−43] Moreover, multimodalities with complex geometries and designs can be incorporated within a single fiber. With the miniature microelectrode enabled by the CNF composite, other functions such as optical waveguides and microfluidic channels can be integrated, which allows for interrogation of neural circuits across their different signaling mechanisms. The techniques and knowledge gained here could shed light on the next generation of microelectrode technology and impact the field of chronic electrophysiology and neuroscience, which will help revolutionize our understanding of how our brain functions as well as extend their potential to neuro-rehabilitative applications in the long term clinical deployment.

METHODS

Synthesis of CNF Composite. The preparation of CNF-loaded electrodes is a multiple step process consisting of dispersing CNFs in commercially available CPE. As a first step, CPE disks of 9 cm diameter and 100 μm thick were cut, individually weighed, and placed on aluminum foil. CNFs were then sprinkled directly on top of the CPE sheets. Each sheet was then weighed and compared to its original weight to deduce the exact amount of CNF deposited on each sheet, and the amount of CNF deposited was adjusted to reach the final objective loading volume content of 2 vol %. In a second step, the CPE disks with deposited CNF were stacked, and the stack was pressed in a hot press at 170 °C and 50 bar for 15 min to embed the CNF into CPE. We obtained a relatively thick CNF-loaded CPE sheet, however at this step the dispersion of CNF was not yet homogeneous. As a control, the sheet was again weighed, and the mass compared to the sum of the masses of the individual CPE disks to deduce once more the exact amount of CNF dispersed and confirmed the 2 vol % loading. The obtained sheet was then chopped into ≈1 mm × 1 mm pieces, and the individual pieces were roughly mixed and pressed again at 170 °C, 50 bar, for 15 min. This created a thick CNF-loaded CPE sheet with a better dispersion of CNF. This disk was then chopped again to form small ≈1 mm × 1 mm granules. The granules were then extruded in a single-screw extruder with a 1 mm circular dye to achieve high-quality mixing of the CNF in CPE into a roughly 1 mm diameter filament. All sections of the extruder (barrel, dye) were preheated at 230 °C, and the screw was run at a speed of 50 rpm. The obtained extruded filament was used as a basis to produce the preform electrodes.

Fiber Fabrication. The extruded CNF composite was compressed with heat into a plate with a thickness of 1 mm. Then the composite electrode was machined into a slab with dimensions of 1 mm × 1 mm × 6 cm. A slot with the same cross-sectional size of 1 mm × 1 mm and a slightly longer length of 6.5 cm, which was intended for the tolerance of the thermal expansion, was machined on the COC slab (TOPAS, Tg 158 °C) with dimensions of 2.5 mm × 2.5 mm × 25 cm. The CNF composite electrode was inserted into the slot of COC slab; another COC slab was placed on top of it and consolidated as a dielectric layer.

DOI: 10.1021/acsnano.6b07550
ACS Nano XXXX, XXX, XXX−XXX

A PC (Mcmaster-Carr, Tg 147 °C) sacrificial cladding layer was used and fabricated by the same process, in order to maintain a miniature footprint for the resulting neural probe as well as to support a stable and controlled drawing. The obtained preform had an overall size with dimensions of 17 mm × 25 mm × 25 cm and then was drawn at temperatures of 150 °C (top), 260 °C (middle), 110 °C (bottom) into a fiber with kilometers long in length using a custom-built fiber drawing tower.

Cross-Sectional and Longitudinal Surface Imaging. Freeze fracture in liquid nitrogen was used to prepare samples of both raw CNF composite prior to the thermal drawing and cross sections of thermally drawn fibers for imaging *via* SEM. Raw CNF composite and fiber sections were fractured by immersion in liquid nitrogen and followed by fragmentation between two grips at low temperature. Exposure of the longitudinal surface of the CNF composite electrode was prepared by immersing the fiber into dichloromethane for 2−3 min to etch away the PC and then in toluene for 2−3 min to etch away the COC.

FIB Milling Process. The CNF composite samples were prepared by etching away the entire polymer cladding layers with dichloromethane and toluene, then a thin layer of platinum (Pt) and palladium (Pd) with a thickness of 8 nm was deposited on the electrode *via* sputtering to avoid electron charge. The sample was mounted in the high-vacuum chamber. The FIB workstation (FEI Helios 600 NanoLab) has dual beams of a high-resolution SEM and an FIB. The sample was located *via* SEM, and the region of interest was centered and tilted into an irradiation angle of 52° that was defined as the angle between the incoming beam and the surface normal. The accelerating voltage and the ion current were set to 30 keV and 93 pA, respectively. A layer of Pt was deposited on top of the region for milling in order to avoid a "curtain effect" and reduce the charging issues of newly exposed areas with polymers. By varying the ion current from 0.92 nA to 0.28 nA to eventually 93 pA, three steps of the Ga ion milling processes were performed from rough milling, fine milling, to final polish. The final milling depth along the transverse direction was 5.5 μm, and the exposed area was 18 μm × 19 μm at the irradiation angle of 52° shown in Figure 3. In another FIB milling experiment, the milling depth was 13 μm, and the exposed area ranged from 15.6 μm × 16 μm to 32 μm × 20 μm as shown in Supplementary Figure 4. In both experiments, multiple images containing aligned CNF in the course of milling were taken *via* SEM.

DC Resistivity Measurement. CNF composite slabs prior to the thermal drawing, which had a cross-section of about 0.52 mm × 2.0 mm and length from 4 cm to 1 cm, were prepared by low-end machining. Thermally drawn fiber sections ranging from 10 cm to 1 cm with the CNF composite of cross-sectional size of 23 μm × 20 μm were also prepared. They were mounted on the probing station (Keithley 4200SCS Parameter Analyzer), two micromanipulators allowed needle probes with radium of 10 μm to point to both terminal cross-section of samples, a DC voltage from −2 V to 2 V with increments of 0.1 V was applied from one end to another, and the resulting DC current was recorded. Then the DC resistance was obtained *via* linear fitting the voltage−current curve, from which the resistivity of CNF composite before and after the thermal drawing was calculated *via* following the Pouillet's law, given the known length and area.

Similarly, fiber sections with CNF composite and CPE, which had a similar size of recording area (25.7 μm × 16.6 μm and 37.2 μm × 14.6 μm, respectively) were chosen and were prepared with a length of 1 cm. Then conductive silver paint (SPI supplies) was applied on both ends to improve the surface contact. The same procedures were performed for measuring the resistivity of the CNF composite and CPE, except that a larger DC scanning range from −15 V to 15 V was used.

Electrochemical Impedance Spectrum (EIS). Fiber sections with CNF composite and CPE having similar cross-sectional size (25.7 μm × 16.6 μm and 37.2 μm × 14.6 μm, respectively) were prepared with a length of 2 cm, and silver paint was then applied at one end to enable the connection with copper wire. Measurements were performed using a potentiostat (Interface 1000E, Gamry Instruments), adopting the both schemes of three-electrode and two-electrode setups within the 1× phosphate buffered saline (PBS) solution. The three-electrode setup was configured with samples as a working electrode, a Ag/AgCl reference electrode (Basi), and a Pt wire as a counter electrode (Basi). 10 mV sinusoidal voltage in the frequency range from 10 Hz to 10 kHz was applied between the reference electrode and the sample against their open circuit voltage, and resulting current was recorded between the sample and the counter electrode, which determined the impedance of the electrode. Measurements with the two-electrode configuration were also performed with the sample as a working electrode and a stainless steel wire (GoodFellow) as reference and counter electrodes, which mimics the electrophysiological experiment in the *in vivo* recording scenario. The same exciting voltage and frequency range for perturbing the electrochemical cell were maintained, and the results, detailed in the material, show the whole impedance of the electrochemical cell.

Assembly of Neural Probes. A fiber section was prepared, and the electrodes were connected to copper wires with conductive silver paint. The wires were then soldered to headpins (Sullins Connector Solutions), along with a stainless steel wire (GoodFellow) as ground reference. Then the fiber tip was immersed in dichloromethane for 2−3 min to remove the PC sacrificial layer, which followed by further cleaning and disinfection in isopropyl alcohol (Sigma) and 70% ethanol (Sigma).

Surgical Procedures. All animal procedures were approved by the Virginia Tech Committee on Animal Care and Use and carried out in accordance with the National Institutes of Health Guide for the Care and Use of Laboratory Animals. Male C57BL/6 mice aged 7−9 weeks (Jackson Laboratory) were used for this study, and all surgeries were conducted under aseptic conditions. Mice were anesthetized by 2−5% isoflurane and positioned in a stereotactic frame (David Kopf Instruments). The scalp was exposed *via* a skin incision, where lambda and bregma points were used to align the skull with respect to a mouse brain atlas. A single implantation was established according to the brain atlas, which was placed in a hippocampal formation (HPF, coordinates relative to bregma; −2 mm anteroposterior (AP); −1.5 mm mediolateral (ML); −1.9 mm dorsoventral (DV)). To facilitate the insertion, the neural probe was coated with melted poly(ethylene glycol) (PEG; 10,000 MW, Sigma). The stainless steel ground wire was soldered to a miniature screw, which was affixed to the skull. The neural probe was fixed to the skull with a layer of superglue and dental cement. Following the surgery and recovery, mice were maintained at 22 °C under 12 h light/dark cycle and provided with food and water *ad libitum*.

***In Vivo* Electrophysiology and Data Analysis.** Electrophysiological recordings were performed by attaching the probes to head stage (PZ5−32, Tucker-Davis Technologies, Inc.) and were acquired using a neurophysiology workstation (RZ5D, Tucker-Davis Technologies, Inc.). The electrophysiological signal was digitized at 25 kHz sampling frequency and filtered in the frequency range of 0.3−5 kHz. Activities including spikes and LFP were detected using custom software written in MATLAB (The Mathworks). Recorded signals were first high-pass filtered from 0.5−5 kHz digitally, and then spikes were detected by setting a voltage threshold and a deadtime of 1 ms to eliminate double detections.[44] The waveform of detected spikes was visually confirmed. Then spike sorting was performed on the detected spikes by classification of them into different clusters *via* K-means clustering. Then sorted clusters were subjected to PCA, furthermore, the L-ratio and isolation distance of the sorted clusters in the first two principal components (PC1-PC2 plane) that accounted for over 90% of the spikes variation[45] were calculated to assess the quality of the separation. LFPs were obtained by digitally filtering the recorded signals from 0.3 to 300 Hz. Then a power spectral density of the LFP was calculated with one-sided fast Fourier transform (FFT).

The interspike interval (ISI) histogram was computed by recording spike times of clustered single-unit action potentials and distributing the intervals into different bin sizes to verify the unit isolation. The autocorrelation of the spikes train was calculated to verify the firing rate pattern of the detected single-unit. Only clusters containing

DOI: 10.1021/acsnano.6b07550
ACS Nano XXXX, XXX, XXX−XXX

<0.015 of the spikes with ISI < 1 ms were considered for further examining the possibility as a single unit.

All analyses are based on customized scripts written in MATLAB and available upon request.

Immunohistochemistry. Animals implanted with a stainless steel probe or a CNF composite probe for 4 weeks were anesthetized with a ketamine (20 mg/mL)/xylazine (2 mg/mL) solution and then transcardially perfused with PBS (Fisher BP661-10), followed by 4% paraformaldehyde (PFA) (Electron Microscopy Sciences cat. no. 15714-S) in PBS. Upon extraction, the brain was kept in 4% PFA overnight at 4 °C and then placed into PBS containing 0.02% sodium azide (Sigma S8032). The brain was serially sectioned into 50 μm transverse slices on a Campden Instruments 5100mz vibratome. All slices were blocked for 1 h at room temperature in blocking solution that contained 10% goat serum (Millipore S26-100 ML) and 0.5% Triton X-100 (Sigma T9284) in PBS. After blocking, slices were incubated with primary antibodies diluted in the blocking solution overnight at 4 °C. Primary antibodies used included chicken anti-GFAP (abcam cat. no. ab4674, 1:1000), mouse anti-NeuN (Millipore cat. no. MAB377, 1:1000), and rabbit anti-Iba1 (Wako cat. no. 019–19741, 1:500). Following primary incubation, slices were washed six times with PBS with 0.1% Tween-20 (Anatrace T1003) (PBST) for 5 min at room temperature with agitation. Secondary antibodies diluted in blocking solution were added at room temperature for 1 h. Secondary antibodies used included goat antichicken Alexa Fluoro 546 (ThermoScientific cat. no. A11040, 1:1000) goat antimouse Alexa Fluoro 488 (ThermoScientific cat. no. A11029, 1:1000) and goat antirabbit Alexa Fluoro 633 (ThermoScientific cat. no. A21070, 1:1000). Slices were then washed six times with PBST for 5 min at room temperature with agitation. Slices were mounted on glass slides with Fluoromount G Mounting Solution (Electron Microscopy Sciences cat. no. 17984–25). Optical sections were acquired using an A1R Nikon laser scanning microscope using a Plan Apo 20×/N.A.0.75 air objective. Quantification of the volumetric data was performed using Imaris 7.5.2 software (Bitplane Scientific Software). Neuron density was calculated by counting NeuN labeled cells using spot detection. Volumetric analysis of GFAP and Iba1 labeled cells was performed on 3D reconstructions created from confocal optical sections.

ASSOCIATED CONTENT

Supporting Information

The Supporting Information is available free of charge on the ACS Publications website at DOI: 10.1021/acsnano.6b07550.

Parameters associated with the drawing process, comparison of thermally drawn CNF composite and CPE electrodes prepared by liquid nitrogen fracture and imaged *via* SEM, images of the exposed inner area of the CNF composite *via* SEM during the course of FIB milling process, the degree of alignment during different drawing stresses, optical images of the drawn fiber sections with CNF composite and CPE electrodes, electrical impedances of thermally drawn CNF composite and CPE, electrochemical impedance measurement of the thermally drawn CNF composite and CPE using two-electrode configuration, principle component analysis of spike clusters at 15 week post-implantation and endogenous activities recorded simultaneously by CPE electrode and CNF composite electrode at the surgical implantation (PDF)

AUTHOR INFORMATION

Corresponding Authors

*E-mail: yuanyuan.guo.a4@tohoku.ac.jp.

*E-mail: xjia@vt.edu.

ORCID

Yuanyuan Guo: 0000-0002-9618-7919

Author Contributions

Y.G., T.Y., and X.J. designed the study. B.G., Y.F., and X.J. designed the CNF polymer composite. Y.G. and B.G. drew the fibers. Y.G. characterized the CNF alignment *via* SEM and FIB. Y.G and S.J. characterized the electrical properties of the composite. Y.G., S.J., and X.J performed the implantation surgeries and recorded the electrophysiological data. Y.G. wrote the MATLAB script and analyzed the recording data. I.F.K., E.G.T., and H.S. performed immunohistochemistry. Y. G. and T. Y. organized data and wrote the manuscript. All authors contributed to the writing of the manuscript and gave their final approval.

Notes

The authors declare no competing financial interest.

ACKNOWLEDGMENTS

The authors gratefully acknowledge the insightful comments and advices from Professor Ko Matsui from Graduate School of Life Science, Dr. Tomomi Tsunematsu from Frontier Research Institute for Interdisciplinary Sciences, and Professor Hajime Mushiake and Dr. Hidenori Watanabe from Graduate School of Medicine at Tohoku University in Japan on the analysis of the electrophysiological signals. We also thank Dr. Blake Johnson from Grado Department of Industrial and Systems Engineering at Virginia Tech for the help with the electrochemical impedance characterization of the electrode. We also acknowledge the Nanoscale Characterization and Fabrication Laboratory in Institute for Critical Technology and Applied Science, Virginia Tech for assistance in materials characterization. Yuanyuan Guo is the recipient of the Japan Society for the Promotion of Science Fellowship (JSPS) for Young Scientist. This work is partially supported by Grant-in-Aid for JSPS research fellows (15J02011). In addition, it was partially supported by the US Army Research Office through the Institute for Soldier Nanotechnologies at Massachusetts Institute of Technology (Contract W911NF-13-D-0001) as well as by MIT MRSEC through the MRSEC Program of the National Science Foundation under award number DMR-1419807.

REFERENCES

(1) Adrian, E. D.; Moruzzi, G. Impulses in the Pyramidal Tract. *J. Physiol.* **1939**, *97*, 153–199.

(2) Strumwasser, F. Long-Term Recording from Single Neurons in Brain of Unrestrained Mammals. *Science* **1958**, *127*, 469–470.

(3) Jog, M. S.; Connolly, C. I.; Kubota, Y.; Iyengar, D. R.; Garrido, L.; Harlan, R.; Graybiel, A. M. Tetrode Technology: Advances in Implantable Hardware, Neuroimaging, and Data Analysis Techniques. *J. Neurosci. Methods* **2002**, *117*, 141–152.

(4) Buzsaki, G. Large-Scale Recording of Neuronal Ensembles. *Nat. Neurosci.* **2004**, *7*, 446–451.

(5) Badi, A. N.; Kertesz, T. R.; Gurgel, R. K.; Shelton, C.; Normann, R. A. Development of a Novel Eighth-Nerve Intraneural Auditory Neuroprosthesis. *Laryngoscope* **2003**, *113*, 833–842.

(6) Wise, K. D.; Angell, J. B.; Starr, A. An Integrated-Circuit Approach to Extracellular Microelectrodes. *IEEE Trans. Biomed. Eng.* **1970**, *BME17*, 238–247.

(7) Bai, Q.; Wise, K. D. Single-Unit Neural Recording with Active Microelectrode Arrays. *IEEE Trans. Biomed. Eng.* **2001**, *48*, 911–920.

(8) Buzsaki, G.; Stark, E.; Berenyi, A.; Khodagholy, D.; Kipke, D. R.; Yoon, E.; Wise, K. D. Tools for Probing Local Circuits: High-Density

DOI: 10.1021/acsnano.6b07550
ACS Nano XXXX, XXX, XXX–XXX

Silicon Probes Combined with Optogenetics. *Neuron* **2015**, *86*, 92–105.
(9) Cheung, K. C. Implantable Microscale Neural Interfaces. *Biomed. Microdevices* **2007**, *9*, 923–938.
(10) Marin, C.; Fernandez, E. Biocompatibility of Intracortical Microelectrodes: Current Status and Future Prospects. *Front. Neuroeng.* **2010**, *3*, 8.
(11) Prasad, A.; Xue, Q. S.; Sankar, V.; Nishida, T.; Shaw, G.; Streit, W. J.; Sanchez, J. C. Comprehensive Characterization and Failure Modes of Tungsten Microwire Arrays in Chronic Neural Implants. *J. Neural Eng.* **2012**, *9*, 056015.
(12) Sankar, V.; Patrick, E.; Dieme, R.; Sanchez, J. C.; Prasad, A.; Nishida, T. Electrode Impedance Analysis of Chronic Tungsten Microwire Neural Implants: Understanding Abiotic *vs.* Biotic Contributions. *Front. Neuroeng.* **2014**, *7*, 13.
(13) Kipke, D. R.; Shain, W.; Buzsaki, G.; Fetz, E.; Henderson, J. M.; Hetke, J. F.; Schalk, G. Advanced Neurotechnologies for Chronic Neural Interfaces: New Horizons and Clinical Opportunities. *J. Neurosci.* **2008**, *28*, 11830–11838.
(14) Pancrazio, J. J.; Peckham, P. H. Neuroprosthetic Devices: How Far Are We from Recovering Movement in Paralyzed Patients? *Expert Rev. Neurother.* **2009**, *9*, 427–430.
(15) Abidian, M. R.; Martin, D. C. Experimental and Theoretical Characterization of Implantable Neural Microelectrodes Modified with Conducting Polymer Nanotubes. *Biomaterials* **2008**, *29*, 1273–1283.
(16) Alba, N. A.; Du, Z. J.; Catt, K. A.; Kozai, T. D.; Cui, X. T. *In Vivo* Electrochemical Analysis of a PEDOT/MWCNT Neural Electrode Coating. *Biosensors* **2015**, *5*, 618–646.
(17) Cui, X. Y.; Lee, V. A.; Raphael, Y.; Wiler, J. A.; Hetke, J. F.; Anderson, D. J.; Martin, D. C. Surface Modification of Neural Recording Electrodes with Conducting Polymer/Biomolecule Blends. *J. Biomed. Mater. Res.* **2001**, *56*, 261–272.
(18) Ludwig, K. A.; Uram, J. D.; Yang, J.; Martin, D. C.; Kipke, D. R. Chronic Neural Recordings Using Silicon Microelectrode Arrays Electrochemically Deposited with a Poly(3,4-Ethylenedioxythiophene) (PEDOT) Film. *J. Neural Eng.* **2006**, *3*, 59–70.
(19) Pierce, A. L.; Sommakia, S.; Rickus, J. L.; Otto, K. J. Thin-Film Silica Sol-Gel Coatings for Neural Microelectrodes. *J. Neurosci. Methods* **2009**, *180*, 106–110.
(20) Kim, J. H.; Kang, G.; Nam, Y.; Choi, Y. K. Surface-Modified Microelectrode Array with Flake Nanostructure for Neural Recording and Stimulation. *Nanotechnology* **2010**, *21*, 085303.
(21) Moxon, K. A.; Kalkhoran, N. M.; Markert, M.; Sambito, M. A.; McKenzie, J. L.; Webster, J. T. Nanostructured Surface Modification of Ceramic-Based Microelectrodes to Enhance Biocompatibility for a Direct Brain-Machine Interface. *IEEE Trans. Biomed. Eng.* **2004**, *51*, 881–889.
(22) Kozai, T. D.; Langhals, N. B.; Patel, P. R.; Deng, X.; Zhang, H.; Smith, K. L.; Lahann, J.; Kotov, N. A.; Kipke, D. R. Ultrasmall Implantable Composite Microelectrodes with Bioactive Surfaces for Chronic Neural Interfaces. *Nat. Mater.* **2012**, *11*, 1065–1073.
(23) Khodagholy, D.; Doublet, T.; Gurfinkel, M.; Quilichini, P.; Ismailova, E.; Leleux, P.; Herve, T.; Sanaur, S.; Bernard, C.; Malliaras, G. G. Highly Conformable Conducting Polymer Electrodes for *In Vivo* Recordings. *Adv. Mater.* **2011**, *23*, H268–H272.
(24) Jan, E.; Hendricks, J. L.; Husaini, V.; Richardson-Burns, S. M.; Sereno, A.; Martin, D. C.; Kotov, N. A. Layered Carbon Nanotube-Polyelectrolyte Electrodes Outperform Traditional Neural Interface Materials. *Nano Lett.* **2009**, *9*, 4012–4018.
(25) Azemi, E.; Stauffer, W. R.; Gostock, M. S.; Lagenaur, C. F.; Cui, X. T. Surface Immobilization of Neural Adhesion Molecule L1 for Improving the Biocompatibility of Chronic Neural Probes: *In Vitro* Characterization. *Acta Biomater.* **2008**, *4*, 1208–1217.
(26) Green, R. A.; Lovell, N. H.; Poole-Warren, L. A. Cell Attachment Functionality of Bioactive Conducting Polymers for Neural Interfaces. *Biomaterials* **2009**, *30*, 3637–3644.
(27) Fu, T. M.; Hong, G. S.; Zhou, T.; Schuhmann, T. G.; Viveros, R. D.; Lieber, C. M. Stable Long-Term Chronic Brain Mapping at the Single-Neuron Level. *Nat. Methods* **2016**, *13*, 875–882.
(28) Xie, C.; Liu, J.; Fu, T. M.; Dai, X. C.; Zhou, W.; Lieber, C. M. Three-Dimensional Macroporous Nanoelectronic Networks as Minimally Invasive Brain Probes. *Nat. Mater.* **2015**, *14*, 1286–1292.
(29) Hong, G.; Fu, T. M.; Zhou, T.; Schuhmann, T. G.; Huang, J.; Lieber, C. M. Syringe Injectable Electronics: Precise Targeted Delivery with Quantitative Input/Output Connectivity. *Nano Lett.* **2015**, *15*, 6979–6984.
(30) Liu, J.; Fu, T. M.; Cheng, Z.; Hong, G.; Zhou, T.; Jin, L.; Duvvuri, M.; Jiang, Z.; Kruskal, P.; Xie, C.; Suo, Z.; Fang, Y.; Lieber, C. M. Syringe-Injectable Electronics. *Nat. Nanotechnol.* **2015**, *10*, 629–636.
(31) Viventi, J.; Kim, D. H.; Moss, J. D.; Kim, Y. S.; Blanco, J. A.; Annetta, N.; Hicks, A.; Xiao, J.; Huang, Y.; Callans, D. J.; Rogers, J. A.; Litt, B. A Conformal, Bio-Interfaced Class of Silicon Electronics for Mapping Cardiac Electrophysiology. *Sci. Transl. Med.* **2010**, *2*, 24ra22.
(32) Viventi, J.; Kim, D. H.; Vigeland, L.; Frechette, E. S.; Blanco, J. A.; Kim, Y. S.; Avrin, A. E.; Tiruvadi, V. R.; Hwang, S. W.; Vanleer, A. C.; Wulsin, D. F.; Davis, K.; Gelber, C. E.; Palmer, L.; Van der Spiegel, J.; Wu, J.; Xiao, J. L.; Huang, Y. G.; Contreras, D.; Rogers, J. A.; et al. Flexible, Foldable, Actively Multiplexed, High-Density Electrode Array for Mapping Brain Activity *In Vivo*. *Nat. Neurosci.* **2011**, *14*, 1599–1605.
(33) Kim, T. I.; McCall, J. G.; Jung, Y. H.; Huang, X.; Siuda, E. R.; Li, Y. H.; Song, J. Z.; Song, Y. M.; Pao, H. A.; Kim, R. H.; Lu, C. F.; Lee, S. D.; Song, I. S.; Shin, G.; Al-Hasani, R.; Kim, S.; Tan, M. P.; Huang, Y. G.; Omenetto, F. G.; Rogers, J. A.; et al. Injectable, Cellular-Scale Optoelectronics with Applications for Wireless Optogenetics. *Science* **2013**, *340*, 211–216.
(34) Canales, A.; Jia, X.; Froriep, U. P.; Koppes, R. A.; Tringides, C. M.; Selvidge, J.; Lu, C.; Hou, C.; Wei, L.; Fink, Y.; Anikeeva, P. Multifunctional Fibers for Simultaneous Optical, Electrical and Chemical Interrogation of Neural Circuits *In Vivo*. *Nat. Biotechnol.* **2015**, *33*, 277–284.
(35) Zhang, D. A.; Rand, E.; Marsh, M.; Andrews, R. J.; Lee, K. H.; Meyyappan, M.; Koehne, J. E. Carbon Nanofiber Electrode for Neurochemical Monitoring. *Mol. Neurobiol.* **2013**, *48*, 380–385.
(36) Zhang, H.; Yu, M.; Xie, L.; Jin, L.; Yu, Z. Carbon-Nanofibers-Based Micro-/Nanodevices for Neural-Electrical and Neural-Chemical Interfaces. *J. Nanomater.* **2012**, *2012*, 1–6.
(37) Yu, Z.; McKnight, T. E.; Ericson, M. N.; Melechko, A. V.; Simpson, M. L.; Morrison, B. Vertically Aligned Carbon Nanofiber Arrays Record Electrophysiological Signals from Hippocampal Slices. *Nano Lett.* **2007**, *7*, 2188–2195.
(38) Buzsaki, G.; Buhl, D. L.; Harris, K. D.; Csicsvari, J.; Czeh, B.; Morozov, A. Hippocampal Network Patterns of Activity in the Mouse. *Neuroscience* **2003**, *116*, 201–211.
(39) Senior, T. J.; Huxter, J. R.; Allen, K.; O'Neill, J.; Csicsvari, J. Gamma Oscillatory Firing Reveals Distinct Populations of Pyramidal Cells in the Ca1 Region of the Hippocampus. *J. Neurosci.* **2008**, *28*, 2274–2286.
(40) Colgin, L. L. Rhythms of the Hippocampal Network. *Nat. Rev. Neurosci.* **2016**, *17*, 239–249.
(41) Boo, H.; Jeong, R. A.; Park, S.; Kim, K. S.; An, K. H.; Lee, Y. H.; Han, J. H.; Kim, H. C.; Chung, T. D. Electrochemical Nanoneedle Biosensor Based on Multiwall Carbon Nanotube. *Anal. Chem.* **2006**, *78*, 617–620.
(42) Huang, J.; Liu, Y.; You, T. Carbon Nanofiber Based Electrochemical Biosensors: A Review. *Anal. Methods* **2010**, *2*, 202–211.
(43) Koehne, J. E.; Marsh, M.; Boakye, A.; Douglas, B.; Kim, I. Y.; Chang, S. Y.; Jang, D. P.; Bennet, K. E.; Kimble, C.; Andrews, R.; Meyyappan, M.; Lee, K. H. Carbon Nanofiber Electrode Array for Electrochemical Detection of Dopamine Using Fast Scan Cyclic Voltammetry. *Analyst* **2011**, *136*, 1802–1805.
(44) Lewicki, M. S. A Review of Methods for Spike Sorting: The Detection and Classification of Neural Action Potentials. *Network: Comput. Neural Syst.* **1998**, *9*, R53–R78.

DOI: 10.1021/acsnano.6b07550
ACS Nano XXXX, XXX, XXX–XXX

(45) Schmitzer-Torbert, N.; Jackson, J.; Henze, D.; Harris, K.; Redish, A. D. Quantitative Measures of Cluster Quality for Use in Extracellular Recordings. *Neuroscience* **2005**, *131*, 1−11.

DOI: 10.1021/acsnano.6b07550
ACS Nano XXXX, XXX, XXX−XXX